

# Observation of wave amplification and temporal topological state in a non-synthetic photonic time crystal

Received: 18 May 2025

Accepted: 31 October 2025

Published online: 17 December 2025

 Check for updatesJiang Xiong<sup>1</sup>, Xudong Zhang<sup>1,2</sup>, Longji Duan<sup>1</sup>, Jiarui Wang<sup>1</sup>, Yang Long<sup>3,4</sup>,  
Haonan Hou<sup>1</sup>, Letian Yu<sup>3</sup>, Linyang Zou<sup>5</sup> & Baile Zhang<sup>3,6</sup>

Photonic time crystals (PTCs) are materials whose dielectric permittivity is periodically modulated in time. Akin to conventional photonic crystals, PTCs give rise to momentum bandgap as well as to topological insulators in the time domain. Here, we experimentally demonstrate the properties of a  $k$  gap in a PTC with real dimensions, realized in a dynamically modulated microwave transmission-line metamaterial. Wave amplification is observed within the  $k$  gap, leading to a narrowing of the initial power spectrum and its shifting toward the gap. To probe the mid-gap topological state, we introduce a temporal interface separating two PTCs with distinct topological phases. The phase difference measured between time-reflected and time-refracted waves at the interface, together with the temporal confinement of the topological state, proves the realization of nontrivial temporal topology. By integrating  $k$  gap amplification with time-domain topological features, our work opens new avenues for light generation and manipulation in time-varying photonic materials.

Crystals generally refer to structures with periodicity in space. In photonics, it has been known since the 1980s that photonic structures with dielectric permittivity periodically modulated in space, commonly referred to as photonic crystals<sup>1–3</sup>, can give rise to photonic bandgaps—frequency ranges where waves cannot propagate but only decay evanescently—similar to the energy bandgaps in semiconductors<sup>4</sup> (Fig. 1a). Inspired by topological insulators<sup>5</sup>, photonic bandgaps have been endowed with topological properties in the past decade, leading to the development of photonic topological insulators<sup>6–8</sup>. As a defining feature, the boundary between two topologically distinct photonic topological insulators hosts topologically protected edge states (Fig. 1b), as determined by the bulk-boundary correspondence, a fundamental principle in topological physics. Taking the simplest one-dimensional (1D) photonic topological insulator<sup>9</sup>

as an example, the existence of an in-gap topological edge state introduces a peak inside the topological bandgap in the wave transmission spectrum through such a 1D system (Fig. 1c).

In a parallel development, the concept of time as an additional dimension of crystallization has been developed in photonic time crystals (PTCs)<sup>10–17</sup>, which are photonic materials whose permittivity varies periodically in time. It has been shown that PTCs can exhibit bandgaps in momentum, known as  $k$  gaps (see Fig. 1d). In contrast to the spatially evanescent modes of conventional photonic bandgaps,  $k$  gaps can host stationary, temporally amplifying modes. Here, the vanishing group velocity accounts for the stationarity, while the non-zero imaginary part of the eigenfrequency drives amplification. When a  $k$  gap is excited through a temporal interface, rather than being spatially reflected, the pulse remains inside the medium with a growing

<sup>1</sup>School of Physics, University of Electronic Science and Technology of China, Chengdu, China. <sup>2</sup>School of Systems Science and Engineering, Sun Yat-sen University, Guangzhou, China. <sup>3</sup>Division of Physics and Applied Physics, School of Physical and Mathematical Sciences, Nanyang Technological University, Singapore, Singapore. <sup>4</sup>School of Physics Science and Engineering, Tongji University, Shanghai, China. <sup>5</sup>School of Electrical and Electronic Engineering, Nanyang Technological University, Singapore, Singapore. <sup>6</sup>Centre for Disruptive Photonic Technologies, Nanyang Technological University, Singapore, Singapore. ✉ e-mail: [linyang001@e.ntu.edu.sg](mailto:linyang001@e.ntu.edu.sg); [blzhang@ntu.edu.sg](mailto:blzhang@ntu.edu.sg)

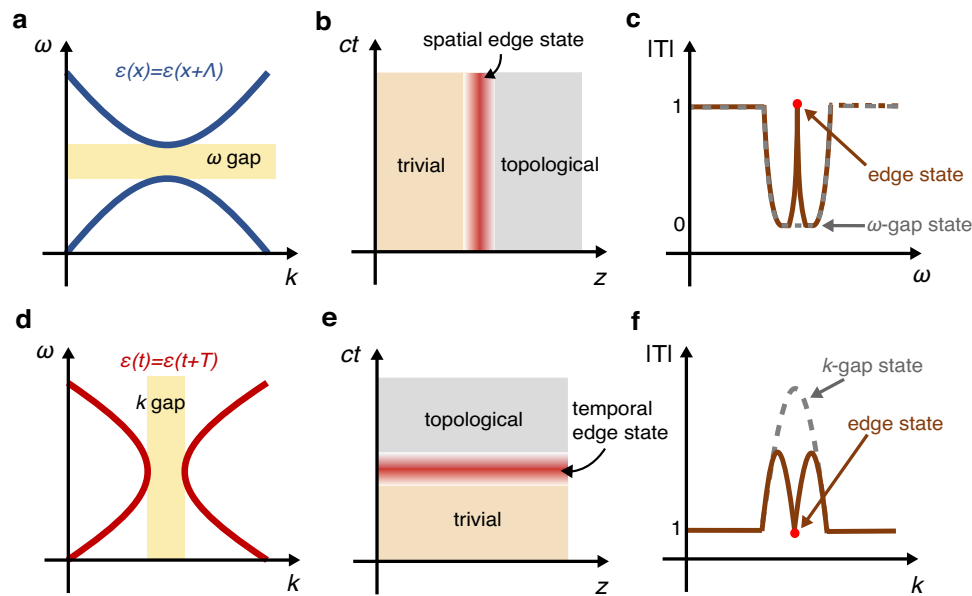


**Fig. 1 | Comparison between a conventional (spatial) photonic crystal and a photonic time crystal. a** Energy bandgap in a spatial photonic crystal. **b** Spatial topological edge state in a 1D spatial topological domain wall. The energy is localized in space while extended in the time domain. **c** (brown) Transmission spectrum of a spatial topological domain wall in (b), where the transmission peak in the bandgap corresponds to the topological edge state. (gray) Transmission spectrum of a pure spatial photonic crystal, in the whole bandgap frequency range most of

the energy is reflected back. **d**  $k$  gap in a photonic time crystal. **e** Temporal topological edge state in a temporal topological domain wall structure. The total energy is localized in time while extended in space. **f** (brown) Transmission spectrum of the temporal topological domain-wall structure in (e) shows a pronounced dip to zero at the mid-gap edge state. (gray) Transmission spectrum of a single photonic time crystal, where the transmitted energy is amplified in the whole  $k$  gap.

temporal amplitude<sup>18</sup>. Such amplification breaks the energy conservation law, thereby greatly differs from a passive slow-light system supporting energy accumulation and field enhancement<sup>19,20</sup>. Moreover, since the spatially uniform modulation and conjugated eigenmodes in  $k$  gap naturally satisfy the phase matching condition<sup>21</sup>, temporal modulation induces non-resonant amplification over the entire  $k$  gap, but is maximized at the mid-gap, providing a mechanism of coherent light generation<sup>22</sup> (e.g., lasers) by drawing energy from time modulation rather than gain media.

Band topology can also be extended to  $k$  gaps in PTCs, giving rise to topological phenomena in the time domain. It has been proposed<sup>18</sup> that a  $k$  gap carries band topology characterized by the Zak phase<sup>23</sup>, a topological invariant used to describe 1D topological insulators. In this context, a nontrivial Zak phase enables a PTC to function as a “temporal” topological insulator. At a temporal interface between two PTCs with distinct Zak phases, a mid-gap temporal edge state can arise in the  $k$  gap (Fig. 1e), analogous to the topological edge state in spatial topological insulators<sup>7</sup>. This temporal topological edge state confines energy in time rather than in space and extends the principle of bulk-boundary correspondence to the time domain. The existence of this in-gap topological state leads to a dip in the transmission spectrum through the 1D system (Fig. 1f). Although temporal localization phenomena were reported in several PT-symmetric platforms<sup>24,25</sup>—where time corresponds to the cycle number of pulses circulating in the coupled fiber loops and space is represented by the relative temporal positions of the pulses within each cycle—as well as in non-photonic systems<sup>26,27</sup>, the direct observation of a temporal topological edge state in a genuine PTC within actual space-time has, until now, remained elusive.

In this work, we present an experimental study of the  $k$ -gap properties in a PTC realized in a dynamically modulated transmission-line metamaterial and metasurfaces<sup>28–31</sup>. We employ a differential modulation strategy, which enables direct observation of the spatio-temporal wave dynamics within the PTC. Moreover, the compact constraints of wave in a microstrip guarantee us to fabricate a sample

with a sufficiently large number of unit cells and consequently permits comprehensive experimental verification of  $k$  gap characteristics. Through space-time Fourier transforms, we capture the temporal band structure, revealing the  $k$  gaps. We demonstrate wave amplification within the  $k$  gap, where an arbitrary initial power spectrum narrows and shifts toward the  $k$ -gap center, confirming the mechanism of coherent light generation via temporal modulation. We then experimentally probe the temporal topology of the  $k$  gap, characterized by the Zak phase, from two perspectives. First, similar to previous studies on 1D photonic topological insulators<sup>9</sup>, the time-reflected and time-refracted waves through the PTC experience different phase shifts, providing clear evidence of the quantized Zak phase. Second, we introduce a temporal interface separating two PTCs with distinct Zak phases. A clear topological state that confines energy in time and induces a dip in the transmission spectrum is observed experimentally. This marks the first experimental observation of a temporal topological edge state in a material platform.

## Results

### PTC Realization and experimental setup

In this work, we employ a microstrip dynamic transmission line (DTL) to realize a PTC, with its geometry detailed in Fig. 2a. Such discrete periodic loading ensures the DTL behaves as a spatially uniform effective medium under DC bias in the long-wavelength regime (effective-homogeneity limit), and accurately mimics a PTC when AC modulation is applied<sup>28,31,32</sup>. The effective permittivity was computed using the field-circuit equivalence<sup>33</sup> across various DC bias levels (Fig. 2b), and the equivalent circuit model of the DTL under the differential modulation scheme is presented in Fig. 2c.

In conventional DTL designs, the transmitting signal along the DTL and the external varactor modulation remain inherently coupled, preventing clear observation of wave temporal dynamics in the realized PTC. To overcome this limitation, we adopt a differential modulation scheme. To achieve precise temporal control over the effective permittivity, we use an arbitrary waveform generator (AWG) to

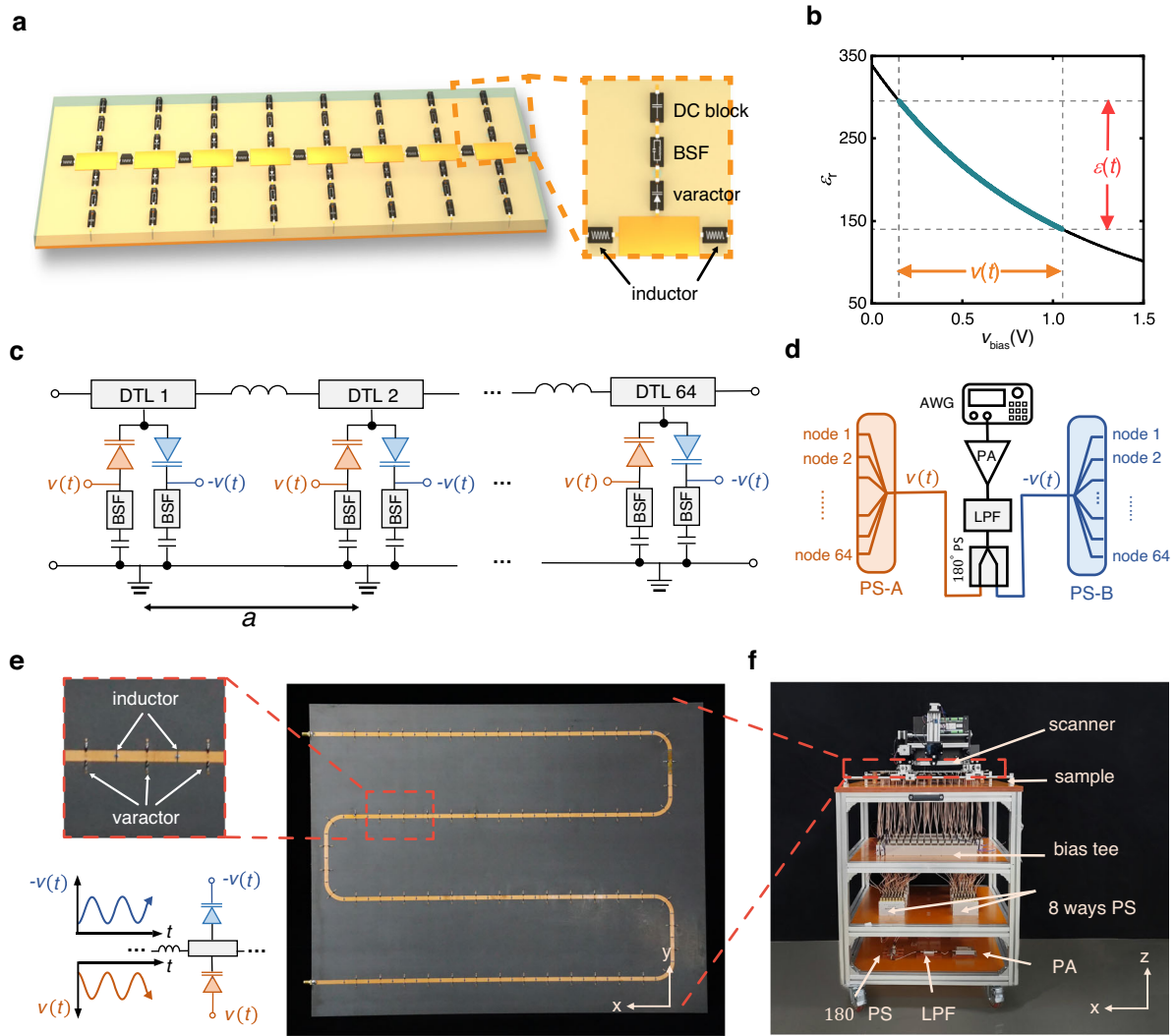


**Fig. 2 | A genuine photonic time crystal implemented in a microwave transmission-line metamaterial.** **a** Schematic view of the dynamic transmission line. It is a microstrip line periodically loaded with shunt varactors and series inductors. The microstrip line applied has a 4.9 mm wide trace line photoetched on a 1.575 mm thick FR4 substrate with dielectric constant  $\epsilon_r = 2.2$  and loss tangent  $\tan\delta = 0.001$  **(b)**  $\epsilon_r$  of the effective medium in **c** at  $\omega = 2\pi \times 65\text{MHz}$  with the varactor bias voltage. The variation spans of a sinusoidal time-varying  $v(t)$  and the resultant quasi-harmonic  $\epsilon_r(t)$  are denoted by orange and red arrows, respectively, and they are both within the relatively linear portion of the curve. **c** Equivalent circuit model for the dynamic transmission-line unit cell and the resultant effective time-varying medium. Symmetric topology is utilized in the equivalent circuit model for the

transmission-line unit cell in **(a)**. **d** Schematic of a three-stage power-dividing network, where the modulation signal is first spitted by a 180-degree phase shifting power divider, and enters two stage 8-way power dividers, finally enter the bias tee for varactor feeding. **e** Fabricated meander-line DTL comprising 64 unit cells. The left inset shows a close-up view, while the schematic below illustrates the corresponding circuit topology for one unit cell, varactor pair positioning with opposite polarity, and the applied out-of-phase time-varying modulation signals. **f** Scaffolding-like measurement platform, showing the 3-stage power dividing network in **d**. A scanner synced with AWG and an oscilloscope is set above the sample for space-time scanning in situ measurement.

produce both the probe and modulation signals (Fig. 2d). The fabricated DTL is presented in Fig. 2e, and the integrated measurement platform is shown in Fig. 2f. This differential modulation scheme, synchronized via an externally generated clock signal, enables direct observation of the genuine spatial-temporal evolution of electromagnetic waves within the time-modulated DTL.

Compared to an infinitely long PTC in theory, any practically realized PTC with finite length has specific spatial boundaries. In this work, the DTL implemented PTC has two terminal ports at both ends, and they affect the experiment in several aspects, as elaborated in Supplementary Note 3. Detailed descriptions of the DTL fabrication, differential modulation circuit, and experimental setup are provided in the Methods section.

### Dispersion and $k$ -gap amplification

We first demonstrate the dispersion of a static DTL. The experimentally extracted band structure of the static DTL is presented in Fig. 3a, with all varactors biased at a DC voltage of 0.6 V. A broadband probe pulse is initially injected into the DTL, and we obtain the static dispersion  $v(\bar{\omega}, \bar{k})$  by a 2D Fourier transform of the recorded spatio-temporal voltage  $v(x_i, t)$  along the meandered line, where  $x_i$  denotes the position index. Throughout this work, frequencies are normalized by the modulation frequency  $\Omega$ , and the wavevector  $k$  is accordingly scaled by the unit wavevector  $k_0 = \sqrt{\epsilon_{eff}}\Omega/c_0$ . A frequency bandgap emerges at  $\bar{\omega} = 1$  as a consequence of the coupling between the transmission line and the periodically loaded BSFs. By modeling the BSFs as effective LC resonators, we numerically calculate the

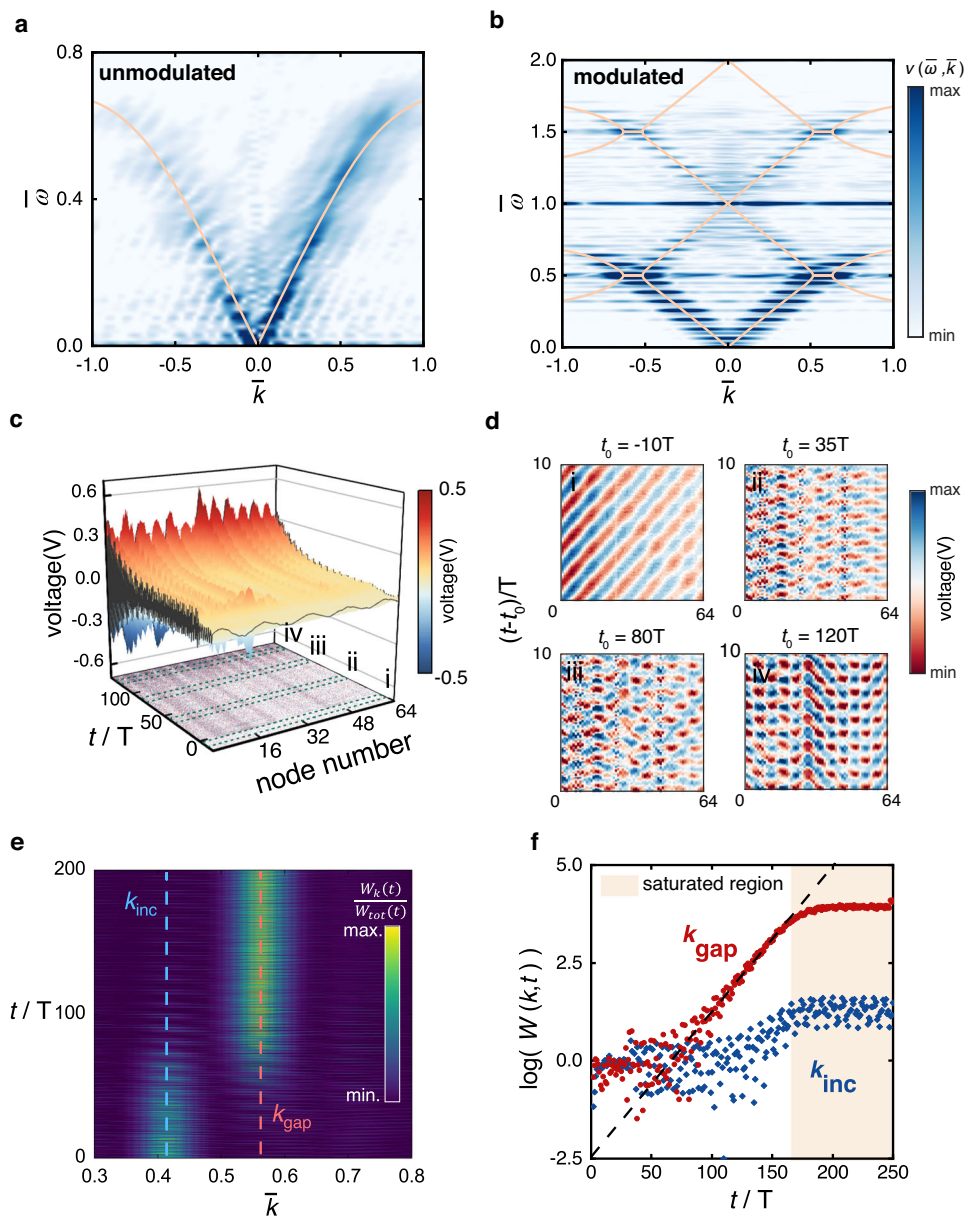


**Fig. 3 | Observation of  $k$ -gap amplification.** **a** Static dispersion of the microstrip line. The heatmap is the normalized band structure of the transmission line with DC bias only, which is obtained via a Fourier transform of the spatiotemporally measured voltage along the line. The frequency is normalized by  $\Omega$ , and the wave number is accordingly scaled by that of a wave propagating in the static line without BSF loading at this frequency. Theoretically calculated dispersion is overlaid on the measured results. **b** Band structures of the DTL when the temporal modulation is added. The heatmap shows the measured normalized band structure, and the theoretical band structures is overlaid as the solid yellow line for comparison.  $k$  gaps open at  $\bar{k} = \pm 0.57$ . **c** Spatiotemporal evolution of the node voltage when excited at  $k$  gaps. **d** Four zoomed in space-time sections in (c) with

their respective starting time labeled as  $t_0$ . The wave in  $k$  gaps exhibits a mode transition from propagating mode to a standing wave profile. **e** Temporal evolution of power spectrum along the DTL when an initial signal of wide spectrum is used for excitation. The momenta at the central frequency of the input signal and the experimentally measured  $k$ -gap center are denoted by blue and red dashed lines, respectively. Note that the power spectrum is normalized by the total power at each moment. **f** Experimentally extracted  $k$  gap and excitation momenta energy evolution in a log scale. The  $k$ -gap mode undergoes exponential growing while the excitation momenta energy remains uniform in time. The orange box indicates the saturation region where the energy stops growing.

dispersion relation<sup>32,33</sup> (solid line in Fig. 3a), which shows good agreement with the measurement. At  $\bar{\omega} = 0.5$ , the dispersion remains linear, ensuring the  $k$ -gap formation in the subsequent modulation.

When the DTL is sinusoidally modulated in time, a PTC and its Floquet bands emerge, with  $k$  gaps open in momentum space. To fully excite the Floquet eigenmode in positive and negative momentum space, we inject a broadband Gaussian pulse train from both ports of the DTL simultaneously. By converting the measured space-time signal into the frequency-momentum domain, we obtain the Floquet band structure shown in Fig. 3b. The measured dispersion reveals two

hallmark features of a PTC: (1) periodic replication of bands along the frequency axis and (2) opening of momentum band gaps at  $\bar{\omega} = 1/2$ . Using the temporal Transfer Matrix Method (TMM)<sup>34</sup> and Floquet theory<sup>35</sup>, the theoretically calculated dispersion relation (yellow solid curves in Fig. 3b) exhibits excellent agreement with the experimental data. Note that we excite the PTC through a temporal interface. As a result, the  $k$ -gap mode, having zero group velocity, remains confined within the transmission line and undergoes self-amplification, producing dark spots in the measured dispersion within the gap region. A horizontal stripe at  $\bar{\omega} = 1$  is attributed to minor leakage of the

modulation signal, which is not fully canceled by the differential modulation scheme. The details of the theoretical calculation are provided in Supplementary Method 2, and a simplified investigation on the system loss impact is provided in Supplementary Discussion 3. The  $k$ -gap modes, by virtue of their non-resonant amplification mechanism, can spontaneously generate coherent standing waves regardless of the input<sup>22</sup>. When a pulse with a broad momentum spectrum is incident on a PTC, it encounters a purely temporal boundary—unlike the spatial boundary of a conventional photonic crystal, which enforces total reflection. Under momentum conservation, all momentum components of the incident wave lying on the original light line map onto the PTC band structure. The momenta in the band region can couple to propagating-wave eigenmodes without experiencing amplification, whereas the momenta within the  $k$  gaps induce exponential amplification, giving rise to standing waves<sup>31,36</sup> and spontaneous formation of spatiotemporal pattern<sup>22,37</sup>. To demonstrate these unique phenomena, we excite the DTL with a quasi-monochromatic wave whose central momenta lies well outside the  $k$  gap. Due to the finite spatial size of DTL, a small fraction of the wave's spatial spectrum leaks into the  $k$ -gap region. We record the full spatial-temporal evolution of the wave in DTL and visualize the dynamics in Fig. 3c. In addition, we also plot in Fig. 3d four space-time sections, each with a different starting time labeled as  $t_0$ , illustrating how the wave evolves under time modulation. Before modulation starts, the incident wave propagates as a traveling wave ( $t_0 = -10T$ ). Once modulation is switched on, amplification occurs and a standing-wave pattern gradually forms ( $t_0 = 120T$ ), accompanied by a reduction in the effective wavelength, confirming dominant momentum conversion. To further analyze the dynamics, we extract the temporal evolution of the normalized spatial power spectrum by applying a spatial Fourier transform at each time step (Fig. 3e). In this figure,  $\bar{k}_{inc}$  and  $\bar{k}_{gap}$  are the normalized momentum at the central frequency of the input signal and that at the  $k$ -gap center, respectively. Even though the input momentum ( $\bar{k}_{inc} = 0.41$ ) lies far away from the  $k$ -gap center ( $\bar{k}_{gap} = 0.57$ ), the  $k$ -gap momenta dominate the power spectrum shortly after the modulation starts, overshadowing all out-of-gap components. Note that this apparent momenta transition arises entirely from the normalization strategy and does not imply a violation of momentum conservation in a PTC. This observation confirms the spontaneous emission behavior of PTCs as predicted theoretically<sup>22</sup>. Additionally, we plot the temporal evolution of the spectral power for both the incident and mid-gap momentum components in log scale (Fig. 3f) and fit them with a straight line, demonstrating the predicted exponential amplification of the  $k$  gap. The small gain of the  $\bar{k}_{inc}$  arises from the spatial truncation and spectral broadening due to the finite size of the DTL. A detailed discussion on this effect is given in Supplementary Discussion 4. It is also worth noting that a discrepancy between the measured result and the perfect exponential growing dashed line becomes apparent after a sufficiently long time (marked in orange in Fig. 3f). We attribute such a saturation to practical limitations in the experimental setup: 1. Finite modulation energy input from power amplifiers. 2. Intrinsic loss in multiple components (DC supply, BSF, etc.). 3. Non-linear capacitance-voltage response at large amplitude. Throughout the measurement, we carefully design the modulation scheme so that all the expected physical events happen long before such saturation emerges.

### Band topology and Zak phase

Interestingly, PTCs also exhibit band topology in the temporal Brillouin zone, characterized by the Zak phase. Firstly, as theoretically established in both PTCs<sup>18</sup> and spatial photonic crystals<sup>9</sup>, in a 1D periodic system with lattice mirror symmetry, the Zak phase of each band is quantized to 0 or  $\pi$ . Furthermore, the sign of a wave scattering observable, i.e., the reflection wave phase for a spatial photonic crystal<sup>9</sup> or the phase difference between the time-reflected and time-

refracted waves for a PTC<sup>18</sup>, can be used to determine the Zak phase of bulk bands. In the context of PTCs, this relation is explicitly given by:

$$\text{sgn}(\varphi_n) = (-1)^{n+l} \exp(i \sum_{m=1}^{n-1} \theta_m^{\text{Zak}}) \quad (1)$$

where  $\varphi_n$  is the phase difference between the time-reflected and time-refracted waves for the  $n^{\text{th}}$   $k$  gap (with the lowest gap number index as 1), evaluated at the last temporal interface between a PTC and the subsequent static medium.  $l$  accounts for the number of band crossings under the  $n^{\text{th}}$  momentum gap ( $l=0$  in our study), and  $\theta_m^{\text{Zak}}$  represents the Zak phase of  $m^{\text{th}}$  band. Note that the term “time-reflected wave” denotes the spatially backward propagation wave caused by a temporal interface via time-modulation<sup>18,29</sup>. We plot in Fig. 4a the temporal profile of both PTCs with distinct Zak phase, where both PTC satisfies the temporal mirror symmetry ( $V(t) = V(-t)$ ) but with opposite symmetry center. When two PTCs with distinct Zak phases are temporally cascaded between a temporal interface (shown by a black dashed line in Fig. 4b), a mid-gap topological edge state emerges inside the  $k$  gap. In our experiment, the sinusoidal modulation opens only the first momentum bandgap. Therefore, we extracted  $\varphi_1$  (referred to simply as  $\varphi$  hereafter) to characterize the  $k$ -gap topology. In the experiment, due to the finite spatial length of the DTL, the momentum resolution inside the  $k$  gap is limited, making it difficult to resolve the intensity/phase spectrum with high precision. To circumvent this issue, we repeat the measurement at different modulation frequencies and effectively increase the number of measurable points in momentum space. Detailed methodology and the phase extraction procedure are described in the Supplementary Method 3 and 4. The experimentally extracted values of  $\varphi$  at nine momenta points in the  $k$  gap are shown in Fig. 4c with blue triangles and red diamonds corresponding to two PTC configurations with  $\theta_1^{\text{Zak}} = 0$  and  $\pi$ , respectively, referred to as PTC1 and PTC2 with opposite temporal lattice mirror symmetry center. The theoretical relation of  $\varphi$  and  $k$  calculated by the Transfer Matrix Method are plotted with blue and red solid lines for comparison. The experimental results agree well with the theory. As expected, PTC1 and PTC2 exhibit the same monotonicity in  $\varphi(k)$  but with opposite signs, highlighting their distinct  $k$ -gap topologies.

### Temporal topological edge state

Finally, we observe the emergence of a temporal edge state at the interface between PTC1 and PTC2. In the context of spatial photonic crystals, it has been demonstrated<sup>9</sup> that the appearance of an unimodular transmission spike at a specific frequency for two photonic crystals with distinct gap topologies ensures a topological edge state confined in space, which is also the point where the summation of the reflection phases of the respective spatial photonic crystals approaches zero. By analogy, a similar phenomenon is expected in the temporal domain: the zero point of the summation of  $\varphi$  for two PTCs with distinct Zak phase (indicated by the black line and dots in Fig. 4c) predicts a critical momenta  $k_c$ , where a temporal topological edge state arises. Unlike that in SPCs, the temporal topological edge state in PTCs manifests as a dip in the total energy spectrum, while the remaining momentum components within the  $k$  gap exhibit high transmission. Both the theoretical (pink solid line) and experimentally extracted (red dot) total energy spectrum are plotted in Fig. 4d. The rationale for adopting total energy  $|T + R|$  instead of transmission  $|T|$  is explained in Supplementary Discussion 1. As expected, a dip appears at  $\bar{k} = 0.564$  in the total energy spectrum, which is close to the theoretical prediction  $k_c$  (marked by dashed green lines in both Fig. 4a, b). Note that owing to the unavoidable loss in the system, the edge state total transmission energy is less than unity. Therefore, for better comparison, we normalize both the theoretical and experimental results by

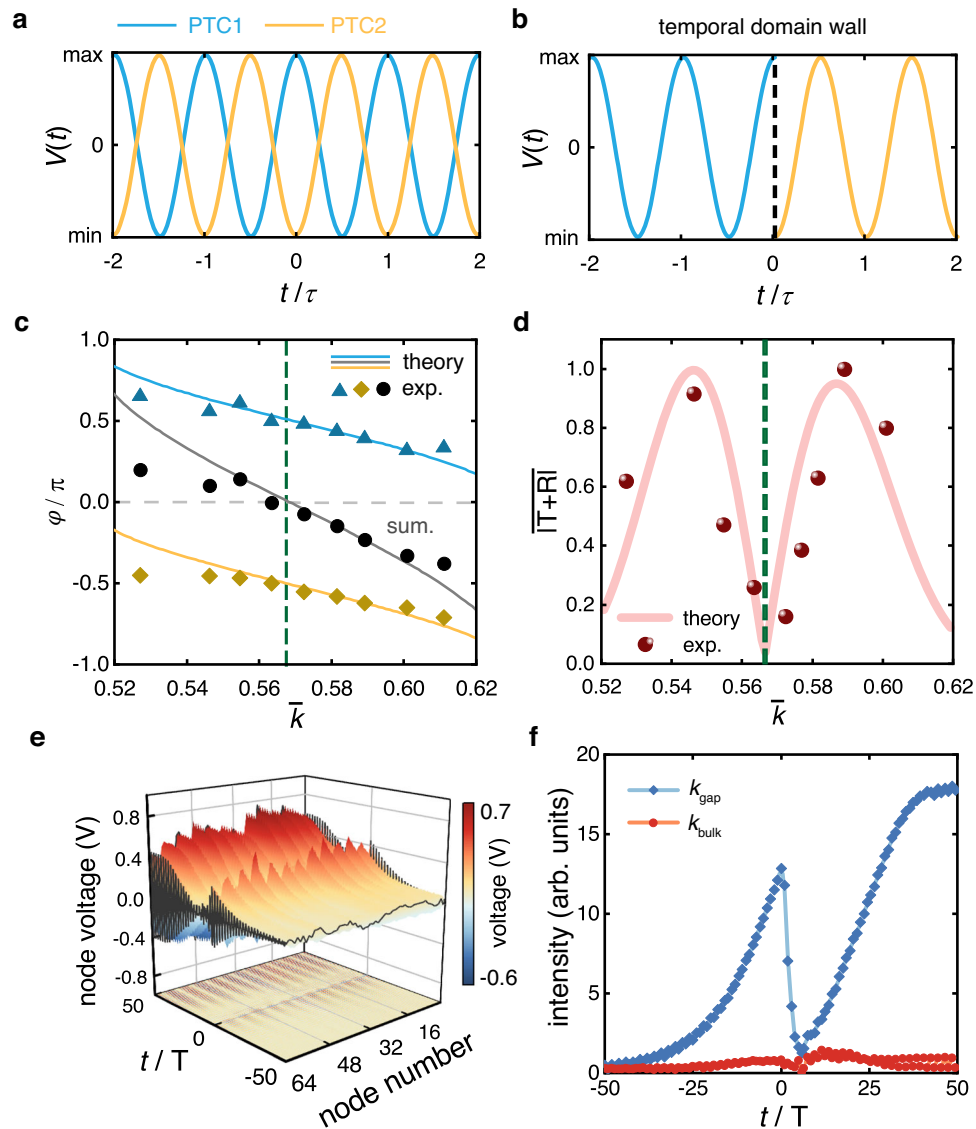


**Fig. 4 | Observation of the temporal topological edge state.** **a** Temporal modulation profile for PTC1 (blue curve) and PTC2 (red curve), exhibiting distinct Zak phase. **b** Temporal domain wall structure by cascading PTC1 and PTC2 in time. At  $t = 0$  a temporal interface is formed (shown by black dash line). **c** Spectrum of the phase difference between the time-transmitted and time-reflected waves inside the  $k$  gap. Two photonic time crystals with identical modulation parameters but an opposite initial modulation phase, denoted as PTC1 and PTC2, are investigated. Experimentally extraction of such a phase difference for PTC1 and PTC2 are plotted with blue triangle and red diamonds. Corresponding theoretically calculated results are plotted with blue and red solid lines for comparison. Phase differences in the two PTCs exhibit the same monotonicity but opposite signs, indicating distinct

topologies. The summation of the two phase differences is plotted with black dots and a solid line, respectively. **d** Experimentally extracted (red dot) and theoretically calculated (red line) normalized total energy spectrum inside the  $k$  gap. A topological edge state appears at the dip in the spectrum, exhibiting unimodal transmission, whose momenta is noted with a green dashed line, same as the green dashed line in (c). **e** Measured space-time field evolution in temporally cascaded photonic time crystals. PTC1 is converted to PTC2 at  $t = 0$ . **f** Temporal evolution of the edge state with  $\bar{k} = 0.5633$  inside the  $k$  gap (blue line) and the bulk state with  $\bar{k} = 0.19$  (red line) in the cascading system in (e). A localized temporal edge state emerges at  $t = 0$  in  $k$  gap, while an extended state is obtained in bulk band.

the maximum value in the  $k$  gap. As a consequence, the normalized edge state transmission is reduced to a close-to-zero value. To probe the associated field dynamics, we excite the DTL at this critical momentum and plot the spatiotemporal field evolution in Fig. 4e. The field shows temporal localization centered at  $t = 0$ , consistent with a temporally localized edge state. We extract the temporal power evolutions of the edge state momenta and plot it in Fig. 4f (blue curve). Prior to the temporal interface between PTC1 and PTC2, the energy exhibits exponential growth as a  $k$ -gap mode. After the temporal switching, the energy undergoes exponential decay, forming a temporal localization profile. This distinct growth-decay pattern constitutes the first direct observation of a temporal topological edge state in a genuine PTC as a material platform. Long after the temporal

switching, the energy is finally re-amplified, which originates from the simultaneous excitation of temporal growth and decaying  $k$ -gap eigenmodes. Note that the temporal asymmetrical growth-decay profile originates from intrinsic losses in the DTL, as also discussed in Supplementary Discussion 3, which suppresses the pre-interface amplification rate and enhances the post-interface decay rate. For comparison, the temporal power evolution of an extended bulk state at  $\bar{k} = 0.19$  is also shown as the red curve in Fig. 4d, rendering a field temporal pattern with a temporally stable magnitude. Field evolutions of several other gap momentum components are also examined and are provided in the Supplementary Discussion 2. Compared to the pronounced temporal localization observed in Fig. 4f, these components exhibit significantly shallower temporal peaks and

correspondingly higher transmission, consistent with their weaker confinement in time.

## Discussion

We have experimentally demonstrated two defining properties of a PTC:  $k$ -gap amplification and temporal topology, both observed in a genuine PTC implemented via a dynamically modulated transmission-line metamaterial platform. The  $k$ -gap amplification reveals a fundamentally distinct mechanism for coherent light generation that circumvents the need for conventional gain media. The temporal topology extends the concept of topological insulators into the time domain, effectively realizing a “temporal” topological insulator. Together, these findings lay the groundwork for future investigations into light–matter interactions in time-varying photonic materials<sup>38,39</sup>—including potential applications in lasing<sup>22,40</sup>—and offer fresh insights into the physics of space–time topological phases<sup>41–44</sup>.

## Methods

### DTL design and fabrication

The photonic time crystal (PTC) was realized using a microstrip dynamic transmission line (DTL) composed of a metallic microstrip trace photoetched onto an FR4 substrate ( $\epsilon_r = 2.2$ ), periodically loaded with 64 pairs of shunt varactors (Skyworks SMV1249-079LF) and series inductors. The varactors provide non-linear, bias-voltage-dependent capacitance, while the inductors are placed to extend the optical path within each unit cell. The modulation was applied within a quasi-linear range (indicated by the blue line in Fig. 2b) to achieve a sinusoidal varying permittivity modulation. Based on critical parameters from the varactor datasheet (including series resistance), typical junction characteristics, and our modulation parameters, the finite time delay caused by carrier transit-time and series resistance effect was estimated to be on the order of picoseconds, which is negligible compared to our 7.7 ns modulation period. Meanwhile, the high-purity MBE-grown varactor exhibits negligible trap-related hysteresis at low frequencies. These considerations regarding varactor latency are supported by prior studies<sup>28,32</sup>.

### Differential modulation scheme

In this scheme, each pair of varactors is reverse-biased with opposite polarities and symmetrically placed on either side of the microstrip trace line in each unit cell. In the equivalent circuit model of DTL (Fig. 2c),  $L_0, C_0$  represent the intrinsic unit-length series inductance and shunt capacitance of the host microstrip line.  $L$  denotes the loaded lumped inductor. Note the blue and orange color varactors have the opposite polarities, and the labels  $v(t)$  and  $-v(t)$  represent the time-varying modulation signal for each varactor diode (see also Fig. 2e). Each varactor is shunted to the ground via a band-stop filter (BSF) resonant at the modulation frequency, thereby isolating the modulation signal. This configuration allows the modulation contributions from each varactor to cancel each other out and leave a clean environment for dynamic signal detection without diminishing the modulation depth.

### Experimental setup and waveform control

An arbitrary waveform generator (AWG) was used to produce both the probe and modulation signals. A three-stage power-dividing network was designed to provide coherent modulation signals for each pair of varactors. The fabricated DTL, integrated with a field scanner and the power dividing network into a compact scaffold-like measurement platform (Fig. 2f). This setup, synchronized via an externally generated clock signal, enabled direct observation of the genuine spatial-temporal evolution of electromagnetic waves within the time-modulated DTL. Additional details on the effective permittivity calculation, experimental setup, and the performance of the differential

modulation are provided in the Supplementary Method 1, Supplementary Note 1 and 2, respectively.

## Data availability

The theoretical and experimental data are available in the data repository for Nanyang Technological University at <https://doi.org/10.21979/N9/2LMCCY>. Other data that support the findings of this study are available from the corresponding authors upon request.

## References

1. John, S. Strong localization of photons in certain disordered dielectric superlattices. *Phys. Rev. Lett.* **58**, 2486–2489 (1987).
2. Yablonovitch, E. Inhibited spontaneous emission in solid-state physics and electronics. *Phys. Rev. Lett.* **58**, 2059–2062 (1987).
3. Fink, Y. et al. A dielectric omnidirectional reflector. *Science* **282**, 1679–1682 (1998).
4. Kittel, C. *Introduction to Solid State Physics*. (Wiley, Hoboken, NJ, 20).
5. Hasan, M. Z. & Kane, C. L. *Colloquium: Topological insulators*. *Rev. Mod. Phys.* **82**, 3045–3067 (2010).
6. Wang, Z., Chong, Y., Joannopoulos, J. D. & Soljačić, M. Observation of unidirectional backscattering-immune topological electromagnetic states. *Nature* **461**, 772–775 (2009).
7. Lu, L., Joannopoulos, J. D. & Soljačić, M. Topological photonics. *Nat. Photon* **8**, 821–829 (2014).
8. Gao, F. et al. Topologically protected refraction of robust kink states in valley photonic crystals. *Nat. Phys.* **14**, 140–144 (2018).
9. Xiao, M., Zhang, Z. Q. & Chan, C. T. Surface impedance and bulk band geometric phases in one-dimensional systems. *Phys. Rev. X* **4**, 021017 (2014).
10. Wang, N., Zhang, Z.-Q. & Chan, C. T. Photonic Floquet media with a complex time-periodic permittivity. *Phys. Rev. B* **98**, 085142 (2018).
11. Sharabi, Y., Lustig, E. & Segev, M. Disordered photonic time crystals. *Phys. Rev. Lett.* **126**, 163902 (2021).
12. Dikopoltsev, A. et al. Light emission by free electrons in photonic time-crystals. *Proc. Natl. Acad. Sci. USA* **119**, e2119705119 (2022).
13. Pan, Y., Cohen, M.-I. & Segev, M. Superluminal  $k$ -gap solitons in nonlinear photonic time crystals. *Phys. Rev. Lett.* **130**, 233801 (2023).
14. Li, H. et al. Stationary charge radiation in anisotropic photonic time crystals. *Phys. Rev. Lett.* **130**, 093803 (2023).
15. Wang, X. et al. Expanding momentum bandgaps in photonic time crystals through resonances. *Nat. Photon.* <https://doi.org/10.1038/s41566-024-01563-3> (2024).
16. Zou, L. et al. Momentum flatband and superluminal propagation in a photonic time Moiré superlattice. Preprint at <https://doi.org/10.48550/arXiv.2411.00215> (2024).
17. Long, Y. et al. Inverse design of topological photonic time crystals via deep learning. *Opt. Mater. Express* **14**, 2032 (2024).
18. Lustig, E., Sharabi, Y. & Segev, M. Topological aspects of photonic time crystals. *Optica* **5**, 1390 (2018).
19. Corcoran, B. et al. Green light emission in silicon through slow-light enhanced third-harmonic generation in photonic-crystal waveguides. *Nat. Photon* **3**, 206–210 (2009).
20. Foteinopoulou, S. & Vigneron, J. P. Extended slow-light field enhancement in positive-index/negative-index heterostructures. *Phys. Rev. B* **88**, 195144 (2013).
21. Slusher, R. E., Hollberg, L. W., Yurke, B., Mertz, J. C. & Valley, J. F. Observation of squeezed states generated by four-wave mixing in an optical cavity. *Phys. Rev. Lett.* **55**, 2409–2412 (1985).
22. Lyubarov, M. et al. Amplified emission and lasing in photonic time crystals. *Science* **377**, 425–428 (2022).
23. Zak, J. Berry’s phase for energy bands in solids. *Phys. Rev. Lett.* **62**, 2747–2750 (1989).

24. Ren, Y. et al. Observation of momentum-gap topology of light at temporal interfaces in a time-synthetic lattice. *Nat. Commun.* **16**, 707 (2025).
25. Feis, J., Weidemann, S., Sheppard, T., Price, H. M. & Szameit, A. Space-time-topological events in photonic quantum walks. *Nat. Photon.* <https://doi.org/10.1038/s41566-025-01653-w> (2025).
26. Li, M.-W. et al. Topological Temporal Boundary States in a Non-Hermitian Spatial Crystal. *Phys. Rev. Lett.* **135**, 187101 (2025).
27. Tong, S. et al. Observation of momentum-band topology in PT-symmetric acoustic Floquet lattices. Preprint at <https://doi.org/10.48550/arXiv.2507.04068> (2025).
28. Reyes-Ayona, J. R. & Halevi, P. Observation of genuine wave vector ( $k$  or  $\beta$ ) gap in a dynamic transmission line and temporal photonic crystals. *Appl. Phys. Lett.* **107**, 074101 (2015).
29. Moussa, H. et al. Observation of temporal reflection and broadband frequency translation at photonic time interfaces. *Nat. Phys.* **19**, 863–868 (2023).
30. Galiffi, E. et al. Broadband coherent wave control through photonic collisions at time interfaces. *Nat. Phys.* **19**, 1703–1708 (2023).
31. Wang, X. et al. Metasurface-based realization of photonic time crystals. *Sci. Adv.* **9**, eadg7541 (2023).
32. Caloz, C. *Electromagnetic Metamaterials: Transmission Line Theory and Microwave Applications: The Engineering Approach* (2010).
33. Pozar, D. M. *Microwave Engineering*. (John Wiley & Sons, Inc, Hoboken, NJ, 2012).
34. Ramaccia, D., Alù, A., Toscano, A. & Bilotti, F. Temporal multilayer structures for designing higher-order transfer functions using time-varying metamaterials. *Appl. Phys. Lett.* **118**, 101901 (2021).
35. Zurita-Sánchez, J. R., Halevi, P. & Cervantes-González, J. C. Reflection and transmission of a wave incident on a slab with a time-periodic dielectric function  $\epsilon(t)$ . *Phys. Rev. A* **79**, 053821 (2009).
36. Lee, S. et al. Parametric oscillation of electromagnetic waves in momentum band gaps of a spatiotemporal crystal. *Photon. Res.* **9**, 142 (2021).
37. Kiselev, E. I. & Pan, Y. Symmetry breaking and spatiotemporal pattern formation in photonic time crystals. *Phys. Rev. A* **111**, 053509 (2025).
38. Galiffi, E. et al. Photonics of time-varying media. *Adv. Photon.* **4**, <https://doi.org/10.1117/1.AP.4.1.014002> (2022).
39. Yin, S., Galiffi, E. & Alù, A. Floquet metamaterials. *eLight* **2**, 8 (2022).
40. Bandres, M. A. et al. Topological insulator laser: Experiments. *Science* **359**, eaar4005 (2018).
41. Kitagawa, T., Berg, E., Rudner, M. & Demler, E. Topological characterization of periodically driven quantum systems. *Phys. Rev. B* **82**, <https://doi.org/10.1103/PhysRevB.82.235114> (2010).
42. Rechtsman, M. C. et al. Photonic Floquet topological insulators. *Nature* **496**, 196–200 (2013).
43. Zhu, W., Xue, H., Gong, J., Chong, Y. & Zhang, B. Time-periodic corner states from Floquet higher-order topology. *Nat. Commun.* **13**, 11 (2022).
44. Weidemann, S., Kremer, M., Longhi, S. & Szameit, A. Topological triple phase transition in non-Hermitian Floquet quasicrystals. *Nature* **601**, 354–359 (2022).

## Acknowledgements

The authors would like to thank Prof. Hao Hu and Mr. Lidong Huang for the helpful discussions, and Chengdu YUEXIANG Technology Co., Ltd

and Chengdu 6914 Technology Co., Ltd for their support in the experiment assembly and technical support in the experiment. Y.L. gratefully acknowledges the support of the Eric and Wendy Schmidt AI in Science Postdoctoral Fellowship, a Schmidt Futures program. This work is supported by the Singapore National Research Foundation Competitive Research Program under Grant No. NRF-CRP23-2019-0007, Singapore Ministry of Education Academic Research Fund Tier 2 under Grant No. MOE-T2EP50123-0007, and Tier 1 Grant No. RG139/22 and RG81/23.

## Author contributions

J.X. conceived the central idea for the experimental setup and led the project. X.Z. and L.D. performed the analytical calculation, carried out the experiment, and conducted the data post processing, assisted by J.W. and H.H. L.Z. proposed the effective measurement methodology, and he also prepared all figures and the manuscript, assisted by J.X., Y.L., and L.Y. B.Z. proposed the motivation and supervised the study. All authors discussed the results and commented on the paper.

## Competing interests

The authors declare no competing interests.

## Additional information

**Supplementary information** The online version contains supplementary material available at <https://doi.org/10.1038/s41467-025-66154-4>.

**Correspondence** and requests for materials should be addressed to Linyang Zou or Baile Zhang.

**Peer review information** *Nature Communications* thanks Mustafa Ozlu, Yihao Yang and the other anonymous reviewer(s) for their contribution to the peer review of this work. A peer review file is available.

**Reprints and permissions information** is available at <http://www.nature.com/reprints>

**Publisher's note** Springer Nature remains neutral with regard to jurisdictional claims in published maps and institutional affiliations.

**Open Access** This article is licensed under a Creative Commons Attribution-NonCommercial-NoDerivatives 4.0 International License, which permits any non-commercial use, sharing, distribution and reproduction in any medium or format, as long as you give appropriate credit to the original author(s) and the source, provide a link to the Creative Commons licence, and indicate if you modified the licensed material. You do not have permission under this licence to share adapted material derived from this article or parts of it. The images or other third party material in this article are included in the article's Creative Commons licence, unless indicated otherwise in a credit line to the material. If material is not included in the article's Creative Commons licence and your intended use is not permitted by statutory regulation or exceeds the permitted use, you will need to obtain permission directly from the copyright holder. To view a copy of this licence, visit <http://creativecommons.org/licenses/by-nc-nd/4.0/>.

© The Author(s) 2025